

Budker Institute of Nuclear Physics

Test of accelerating section for VEPP 5 pre injector

M.S. Avilov, V.E. Akimov, A.V. Aleksandrov, A.V. Antoshin,
P.A. Bak, O.Yu. Bazhenov, Yu.M. Boimelshtein, D.Yu. Bolkhovityanov,
R.Kh. Galimov, R.G. Gromov, K.V. Gubin, S.M. Gurov, Ye.A. Gusev,
N.S. Dikansky, N.I. Zinevich, I.V. Kazarezov, N.A. Kiseleva,
V.I. Kokoulin, V.I. Kopylov, S.N. Klyushev, M.B. Korabelnikov,
A.A. Korepanov, A.N. Kosarev, N.Kh. Kot, N.N. Lebedev, P.V. Logatchev,
A.N. Lukin, P.V. Martyshkin, L.A. Mironenko, A.A. Nikiforov,
A.V. Novokhatski, V.M. Pavlov, I.L. Pivovarov, O.V. Pirogov,
V.V. Podlevskikh, S.L. Samoilov, B.A. Skarbo, B.M. Smirnov,
A.N. Skrinsky, A.N. Sudarkin, D.P. Sukhanov, A.R. Frolov,
A.S. Tsyganov, A.G. Chupyra, V.D. Khambikov, V.D. Shemelin,
S.V. Shiyankov, Yu.V. Yudin.

BUDKERINP 2000 50

**NOVOSIBIRSK
2000**

Test of accelerating Section for VEPP 5 Pre injector

*M.S. Avilov, V.E. Akimov, A.V. Aleksandrov, A.V. Antoshin,
P.A. Bak, O.Yu. Bazhenov, Yu.M. Boimelshtein, D.Yu. Bolkhovityanov,
R.Kh. Galimov, R.G. Gromov, K.V. Gubin, S.M. Gurov, Ye.A. Gusev,
N.S. Dikansky, N.I. Zinevich, I.V. Kazarezov, N.A. Kiseleva,
V.I. Kokoulin, V.I. Kopylov, S.N. Klyushev, M.B. Korabelnikov,
A.A. Korepanov, A.N. Kosarev, N.Kh. Kot, N.N. Lebedev, P.V. Logatchev,
A.N. Lukin, P.V. Martyshkin, L.A. Mironenko, A.A. Nikiforov,
A.V. Novokhatski, V.M. Pavlov, I.L. Pivovarov, O.V. Pirogov,
V.V. Podlevskikh, S.L. Samoïlov, B.A. Skarbo, B.M. Smirnov,
A.N. Skrinsky, A.N. Sudarkin, D.P. Sukhanov, A.R. Frolov,
A.S. Tsyganov, A.G. Chupyra, V.D. Khambikov, V.D. Shemelin,
S.V. Shiyankov, Yu.V. Yudin.*

Budker INP,

630090 Novosibirsk, Russian federation

Abstract

Basic results of VEPP 5 pre injector accelerating section tests are presented in this paper. Single 3 m long accelerating section was powered by 240 MW RF of 5045 klystron with pulse compression system.

The maximum beam energy of 105 MeV was detected at U turn magnetic spectrometer. The beam energy per pulse 26 J was reached at the energy of 92 MeV for the 310 ns beam current.

Introduction

The accelerating channel of VEPP 5 pre injector consists of two linear accelerators for the energy 300 MeV and 510 MeV and contains of 14 accelerating sections (AS) [1,2]. First accelerator sections of both linacs have the increased accelerating gradient 25 30 MeV/m, while the others have 17 20 MeV/m. The goal of presented tests is the experimental check out of AS operation at the maximum possible acceleration and at different beam current.

Tests were carried out on the basis of initial part of pre injector (first accelerating assembly) that includes an electron gun, subharmonic buncher, S band buncher, three accelerating sections, RF assembly on the basis of 5045 SLAC klystron, a pulse compression system, focusing system and a system of beam diagnostics. To get the maximum accelerating, all RF power after the compression is directed into the first accelerating section. The rest two sections and the subharmonic buncher were out of operation in present experiments and were used as the channel of beam transportation. Moreover, at the present regime of section operational conditions, the electron accelerator operation was simulated for intensive source of resonant neutrons (IREN), following the agreement with JINR, Dubna [3].

Accelerating Section

The accelerating section (AS) of VEPP 5 pre injector (Fig. 1.) is managed as the cut of a round disk loaded waveguide with the constant impedance (the constant cell geometry along the AS). Two wave type transformers (WTT) are placed at the input and the output of the section. WTT transforms the basic mode of waveguide channel H_{10} into the accelerating mode E_{01} of a round disk

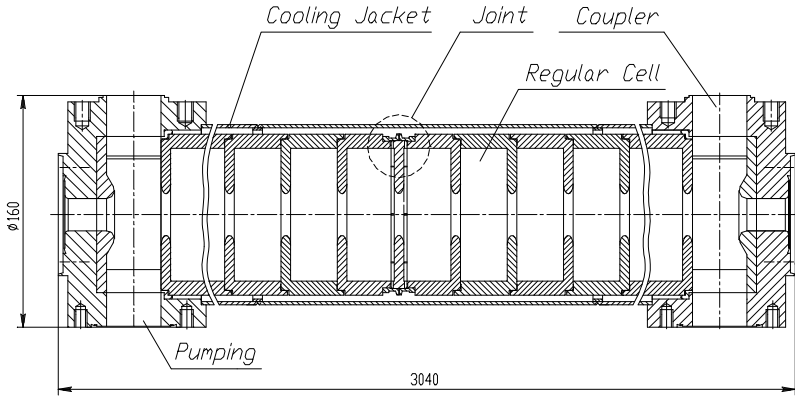


Fig. 1. Accelerating section.

loaded waveguide. To reduce the overvoltage ratio, the edge of the iris is performed as an ellipse with the half axis ratio 1:2 (see Fig. 2).

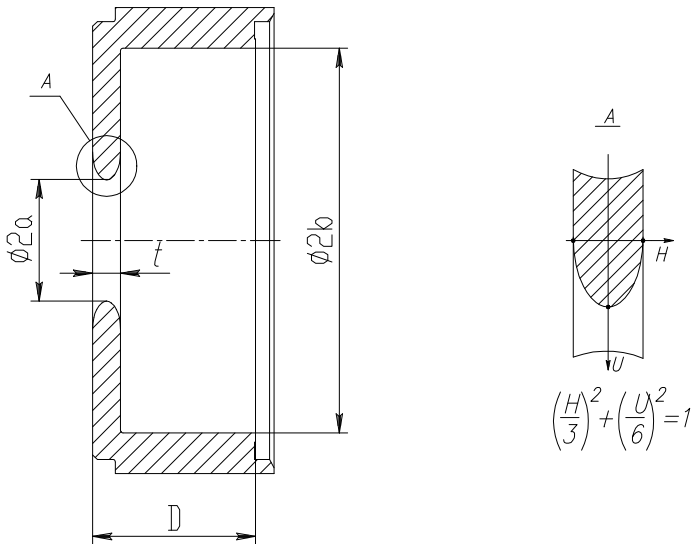


Fig. 2. Geometry of accelerating section's cell.

During the process of section manufacture the resonant frequency control of the test bed, that was assembled of two regular cells (one of it is measured), and two half cells with the exciting and receiving antennas, is carried out. By the results of measurements the selection of cells by frequency and group velocity was carried out and then cells were assembled on the special test bed. After the assembly the measurement of RF signal reflected from AS were carried out as well as RF power dissipation in the section. The section was matched with the waveguide channel in order to achieve the minimum reflection at the operating frequency. The matching was provided by the tuning of WTT. The tuning was carried out by the change of WTT inlet size, diameter of WTT cavity, and size of ring lug around the vacuum channel inlet. The section was assembled of two identical parts of 1.5 m length each. Brazing of each part was carried out in the vacuum furnace. After AS brazing the measurements were repeated. Both brazed half sections were welded together via the connecting iris, as shown in Fig.3.

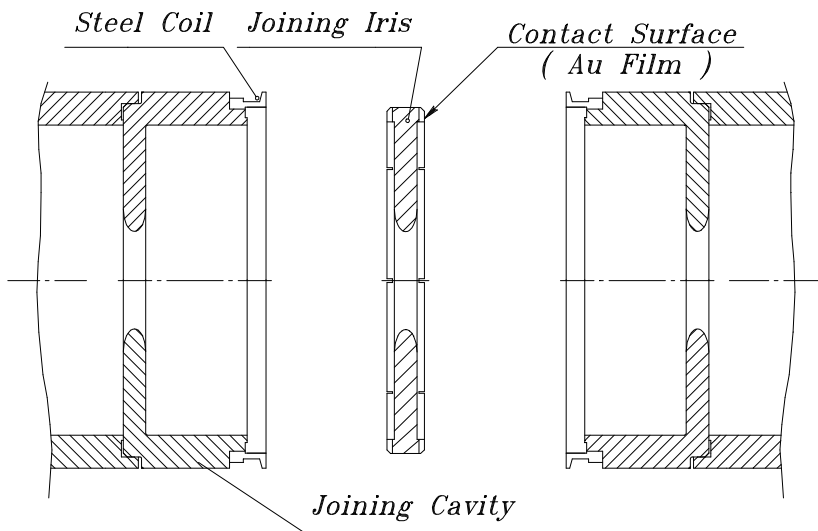


Fig. 3. Connection of two AS parts.

Sides of connecting iris were covered by the golden film. The iris was tightened between the special connecting cells up to formation of the thermal diffusion seam. Then, in order to provide the vacuum, the welding of steel rings was done. The AS parameters are presented in Table 1.

Table1. Parameters of the accelerating section.

Operational frequency	2855.5 MHz
Internal cell diameter $2b$	83.75 mm
Iris diameter $2a$	25.9 mm
Iris thickness t	6 mm
Period D	34.99 mm
Operational mode of oscillation θ	$2\pi/3$
Relative phase velocity β_p	1
Relative group velocity β_g	0.021
Section length L	2.93 m
Total number of cells (incl. 2 WTT)	85
Unloaded quality factor Q_0	13200
Shunt impedance R_{sh}	51 MOhm/m
Time constant $\tau_{0a}=2Q_0/\omega_0$	1.471 μ s
Attenuation (by field) $\alpha=1/(\tau_{0a}v_{gr})$	0.108 m ⁻¹
Filling time $T_f=L/v_{gr}$	0.465 μ s

Before the experiments, the AS and all waveguide channel were backed for 3 days at the temperature 230°C. The vacuum of $\sim 3 \cdot 10^9$ Torr was achieved after the backing and RF processing.

The scheme of RF test is shown in Fig.4.

RF Power Supply of the Assembly

The continuous RF signal ($f = 1428$ MHz, $P \approx 10$ mW) from the master oscillator is directed to the shaping amplifier assembly U2856 2 via 90° phase shifter. The shaping amplifier operates at the doubled frequency 2856 MHz and forms the RF pulse of ~ 3.5 μ s width and output pulsed power of 200÷400 W for 5045 klystron excitation. Phase shifter provides the phase inversion at the operational frequency at the given time moment to ensure the pulse compression system operation. RF pulse of up to 60 MW power is moved from the klystron through the waveguide channel (72 x 34 mm²), SLED type pulse compression system, to the AS input. The unused power in the AS is dissipated in the dummy load, which is located at the output of the section. The fraction of RF power after SLED system is directed to the RF buncher via the directional coupler with the attenuation of $\alpha_c = 23$ dB. RF phase and amplitude can be varied by the attenuator and phase shifter.

For RF power supply operation control using of waveguide to coaxial direct

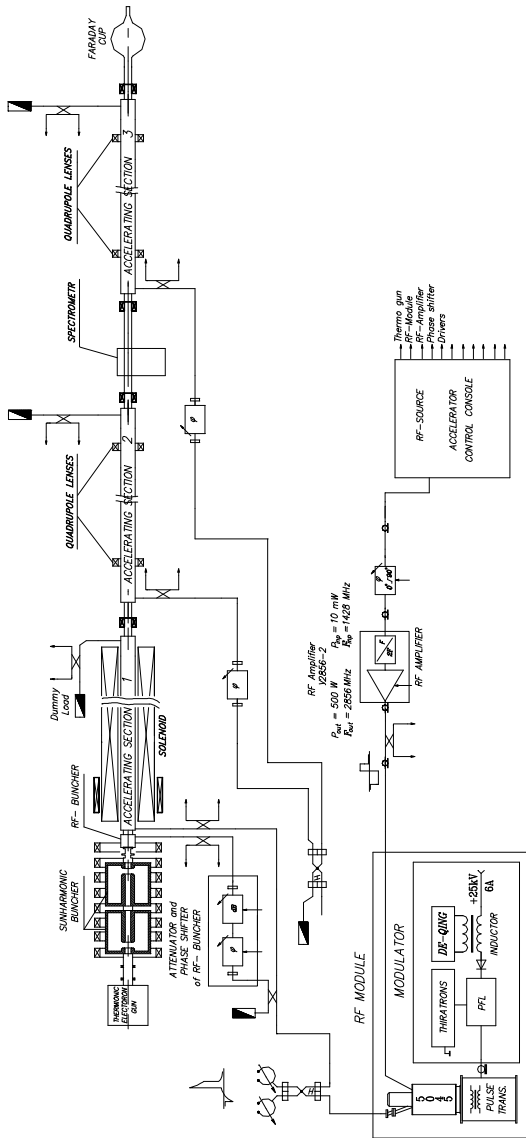


Fig. 4 The scheme of RF test.

couplers, the following RF signals were measured:

- incident wave amplitude at the input of 5045 klystron;
- incident and reflected wave amplitudes after the klystron (before the power compression system);
- incident and reflected wave amplitude at the buncher input;
- incident and reflected wave amplitude at the AS input;
- relative phase shift between the RF buncher and the AS;
- level of incident and reflected power directed to the load.

System of power compression SLED (see Fig.5) consists of waveguide gap coupler and two cylindrical cavities with high quality factor. Operation mode of cavities H_{015} .

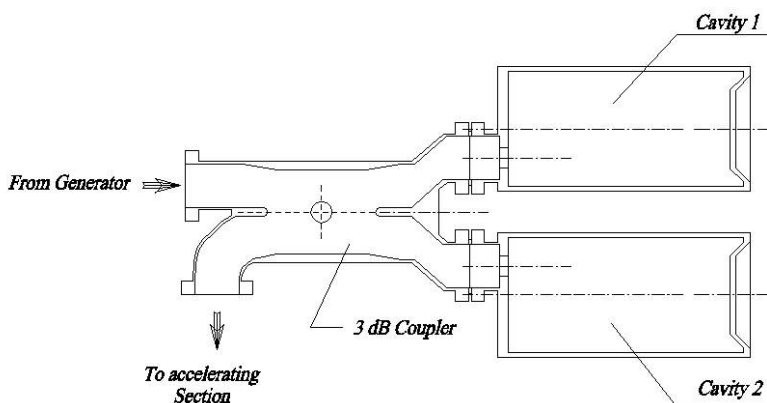


Fig. 5. Pulse compression system SLED.

One of the cavity wall is mobile, that provides operational tuning of power compression system using step driver. The low power test of cavity parameters were preliminary done (see Tab.2).

RF Buncher

For preliminary beam bunching, the RF buncher is set at the AS input. The buncher design is shown in Fig.6. It consists of four coupled cylindrical cavities (three cells + WTT).

Table 2. Parameters of power compression system cavities.

Cavity diameter D		196 mm
Cavity height H		346.9 mm
Operational frequency f_0		2856 MHz
Frequency tuning range	Δf	± 5 MHz
	$\Delta f/\Delta H$	2.75 MHz/mm
Unloaded quality factor Q_0		86200
Coupling ratio with waveguide β		9.8
Cavity time constant $\tau_0 = 2 Q_0/\omega_0$		9.6 μ s
Loaded cavity time constant $T_c = \tau_0/(1 + \beta)$		0.9 μ s

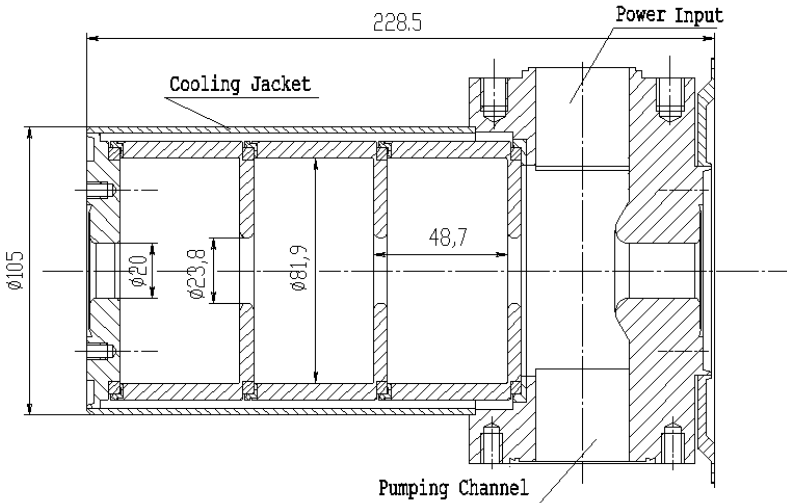


Fig. 6. RF buncher design .

The buncher is fabricated of relatively high surface resistance material stainless steel 12X18H10T type. The jacket is available to provide cooling and thermostabilization. The pumping is carried out via the hole located opposite the power input, that forms the symmetrical electric field in the first cell. The buncher parameters are presented in Tab.3.

Table 3. RF buncher parameters.

Internal cell diameter $2b$	81.9 mm
Iris diameter $2a$	23.8 mm
Iris thickness t	5 mm
Period D	48.7 mm
Resonant frequencies: f_1	2831.48 MHz
f_2	2841.92 MHz
(operational frequency) $f_{0g} = f_3$	2856.45 MHz
f_4	2866.84 MHz
Unloaded quality factor at f_{0g} frequency Q_{0g}	3350
Operational mode of oscillation θ	$4\pi/3$
Relative phase velocity β_p	0.695

System of Thermostabilization

The control of AS temperature, load, RF buncher and SLED cavities is provided by the system of thermostabilization. The stabilization of temperature is ensured by change of cooling distilled water temperature at the input of cooling system. The parameters of system of thermostabilization are presented in Tab.4.

Table 4. Parameters of system of thermostabilization.

Operational water consumption	0.2 0.5 l ps
Consumption stability	$\pm 10\%$
Operational temperature range	25 40°C
Operational temperature	30°C
Accuracy of temperature stabilization	$\pm 0.1^\circ\text{C}$
Power consumption	up to 20 kW

High Voltage Electron Gun

The three electrode thermionic gun with the oxide cathode is used as a source of electrons [3]. Main e gun parameters are presented in Tab.5.

Table 5. Main parameters of the electron gun.

Electron gun voltage	up to 200 kV
Current pulse width (FWHM)	2÷350 ns
Pulsed current	up to 3 A
Repetition rate	up to 50 Hz

Focusing System

The focusing system of first accelerating assembly consists of 6 lenses, 6 coils (diameter is of 525 mm, current up to 510 A) and three sectional solenoid (internal diameter is of 174 mm, external diameter is of 371 mm, total length is of 2210 mm, current up to 1100 A).

To steer the beam from AS to magnetic spectrometer and Faraday cup, quadrupole doublets are used. The beam rays is corrected by magnetic correctors located in the accelerating channel.

The control system enables the fast current change of any focusing system element.

Beam Diagnostics System

System of beam diagnostics includes the measurements of following beam parameters: pulsed current and total charge of the beam from the electron gun, charge and energy characteristics of accelerated beam and also its position at input and output of AS.

Gun pulsed current is measured by the wall current monitor located at the gun output.

Measurements of beam energy characteristics are made by 180° magnetic spectrometer. After spectrometer the beam was directed to the luminescent screen. One can define the energy of accelerated electrons by spectrometer magnetic field strength and radius of particles turn. Also the beam energy spread can be evaluated by the beam spot size and relative brightness on the luminescent screen. The ratio between the spectrometer magnetic field strength and magnetic coils current was preliminary measured. After measurements the beam energy within the current range 1700÷2100 A was defined as:

$$U[\text{MeV}] = 1.62 \frac{I[\text{A}]}{2100} D[\text{cm}],$$

where I is current of spectrometer coils, D is beam turn diameter. Total error of the beam energy definition is a sum of beam turn diameter definition error and hysteresis of magnetic field due to spectrometer magnet switching, one is equal of $\pm 3\%$. The charge of accelerated beam is measured by the Faraday cup, which is located after the luminescent screen.

The beam position at the input of the accelerating section was controlled by the luminescent screen at the input of AS, and by the band type two coordinate pick up at the AS output.

Results of Measurements with the Short Bunch

The pulsed electron current injected in the section was about of 3 A at the pulse width 2 ns. For this pulse width the beam radiation field is low and doesn't influence essentially on the acceleration. The accelerating field of the AS is depended on the klystron input power only. At that operational conditions it is possible to reach the maximum accelerating gradient and, hence, the maximum energy of the accelerated beam.

The operational RF pulse at the input and the output of pulse compression system (input of AS) is shown in Fig. 7.

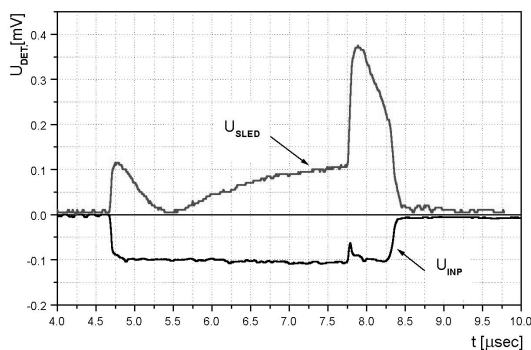


Fig. 7. RF pulse shape at the input and output of power compression system.

As example, RF pulses obtained during the AS training at the moments of breakdown, are shown in Fig.8.

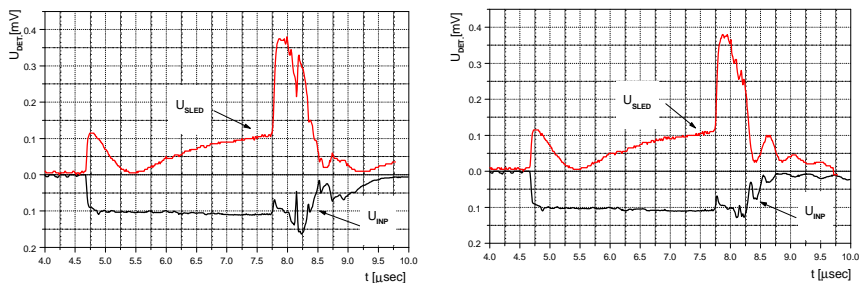


Fig.8. RF pulse shape at the input and output of pulse compression system at the breakdown.

The operational parameters of power compression system cavities are calculated, using the method of regressive analysis and the RF pulse shape after the power compression system:

unloaded quality factor	$Q_0 = 7.58 \cdot 10^4$;
time constant	$\tau_0 = 8.45 \mu\text{s}$;
coupling ratio with the waveguide channel	$\beta = 8.2$;
time constant of loaded cavities	$T_c = \frac{\tau_0}{1 + \beta} = 0.92 \mu\text{s}$;

and also typical times of input signal transient processes:

$\tau_1 = 0.021 \mu\text{s}$ - typical time of growth of incident wave amplitude leading pulse edge;

$\tau_2 = 0.044 \mu\text{s}$ - typical time of phase inversion.

As example, the pulse shape after the power compression system at pulsed input power amplitude $P_{inp} = 50 \text{ MW}$ is shown in Fig.9.

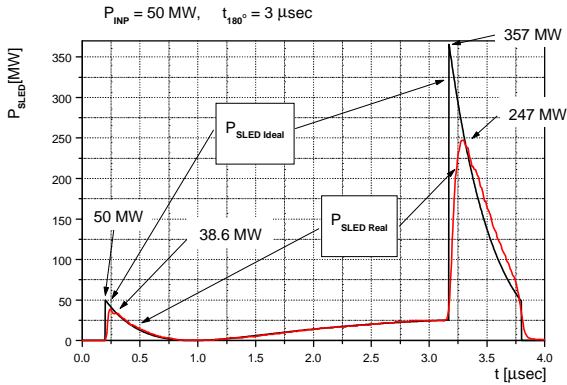


Fig.9. Power pulse shape after pulse compression system.

One can calculate the distribution of accelerating electric field amplitude along the AS at different instants by the shape of RF pulse at the AS input and AS parameters. For constant impedance structure

$$E(z, t) = E_0 \left(t - \frac{z}{v_{gr}} \right) e^{-\alpha z},$$

where $E_0(t) = E(0, t)$ is electric field amplitude at the AS input at $z=0$.

The accelerating field distributions vs. z coordinate along the section at different instants t , calculated by the realistic shape of RF pulse (Fig.9) are shown in Fig.10.

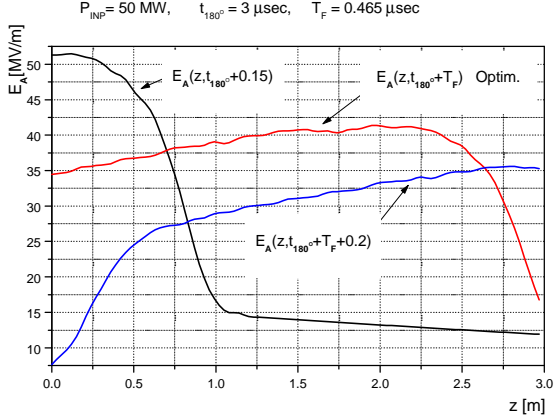


Fig. 10. Accelerating field distribution along the AS at different time.

The energy gain of the accelerated particle that enter the AS at time t , when $v_{gr} \ll c$ (i.e. the particle instantly passed the AS),

$$U(t) = e \int_0^L E(z, t) dz .$$

Since at different moments of particle entrance in the AS the RF energy filling is different, then the beam passed the AS has different energy gain depending on its moment of entrance in the AS. The dependence of beam energy W_{out} on the moment of entrance t in the AS is shown in Fig. 11.

At present time the short accelerated beam with $2 \cdot 10^{10}$ particles in the bunch is obtained at the output of the first AS. Maximum average accelerated gradient 35 MeV/m is reached. As it is seen in Fig.10, the maximum amplitude of accelerating field in first cells is 50 MV/m.

The AS operated at 5 Hz repetition rate (output energy of electrons 106 MeV) with a single breakdown during 40 minutes of operation, and without any breakdown at 50 Hz repetition rate (output energy 75 MeV). The photos of luminescent screen for accelerator operations with the RF buncher switched on and off are presented in Fig. 12 13.

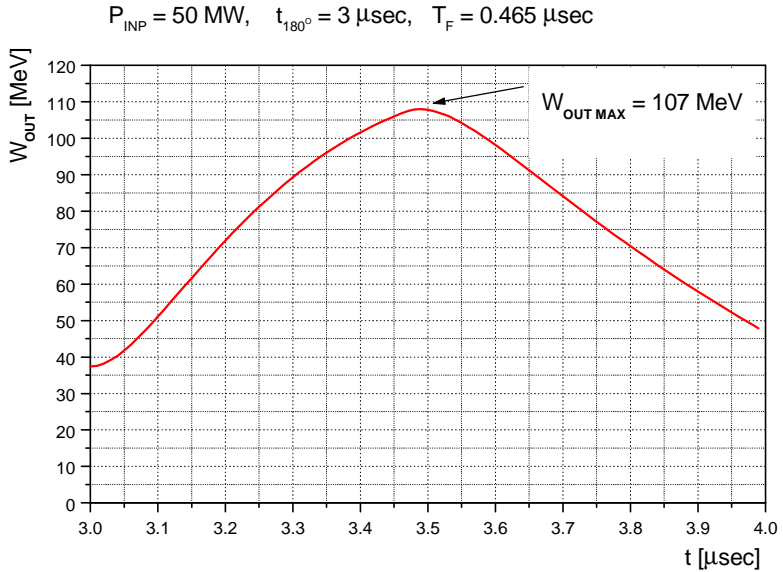


Fig. 11 Beam energy vs. moment of entrance in the AS.

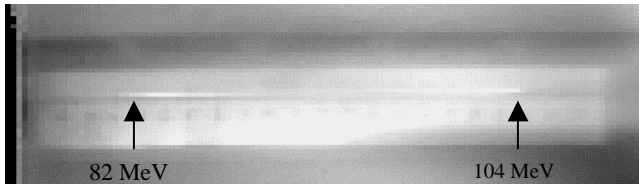


Fig.12. Accelerated beam with RF buncher switched off.



Fig.13. Accelerated beam with RF buncher switched on.

When the RF buncher was switched on, the energy spread in the beam was $\pm 0.5 \%$.

Results and Analysis of Experiments with Long Bunch

The goal of these experiments was the AS test at the conditions close to operational of the accelerator project for IREN [3], namely, the injected current is not less than 1.5 A for the pulse width ≈ 250 ns. This bunch duration is already the same as the duration of operational part of RF pulse. At these conditions the AS operates with strong current load that leads to essential change of the AS accelerating field and accelerated beam characteristics. These conditions are typical for the beam with high energy capacity.

Test conditions were:

repetition rate	$F = 1 \div 5$ Hz;
electron gun voltage	$U = 170$ kV;
gun pulsed current	$I_G = 2.6$ A;
current pulse width	$\tau_b = 310$ ns;
output klystron power	$P_{kl} \approx 50$ MW;
RF pulse width	$\tau_{kl} = 3.6$ μ s;
time before phase inversion	$t_{180^\circ} = 2.83$ μ s.

Except the signals listed above in the present series of experiments the next parameters were also measured:

1. Current pulse from the wall current monitor at the electron gun output.
2. Signals from beam parameters controller (BPC) at the output of magnetic spectrometer. The controller is performed as a set of charge collections with capacity 5.8 nF each, and allows to measure the charge with the energy resolution ≈ 1.8 MeV.

Signals from detector heads and BPC were digitized by ADC with time resolution 10 ns, stored for further procession and monitored on the control computer display.

In that experiment RF buncher wasn't fed by the power and unbunched beam was steered to the AS input, that is why the accelerated beam had large energy spread. The photo of luminescent screen before BPC was put into operation is shown in Fig 14, and the signal from BPC the dependence of particle density on the energy is shown in Fig.15. The density corresponded to the maximum of energy capacity.

Maximum electron energy of the accelerated beam is 92 MeV, minimum is 47 MeV, total beam charge is of $1.52 \cdot 10^7$ Coulomb (total number of particles $N_e = Q/e = 9.52 \cdot 10^{11}$). One can calculate the beam total energy capacity by the particle density distribution and energy:

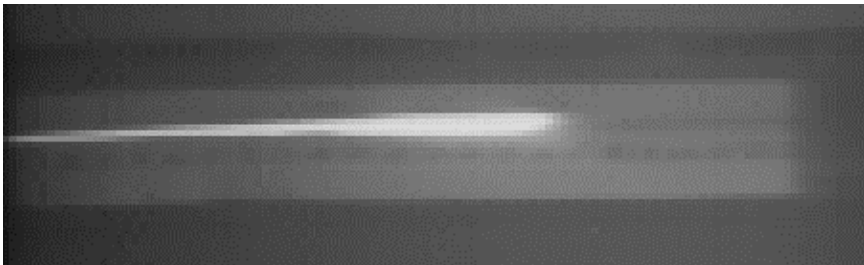


Fig.14. Photo of accelerated beam.

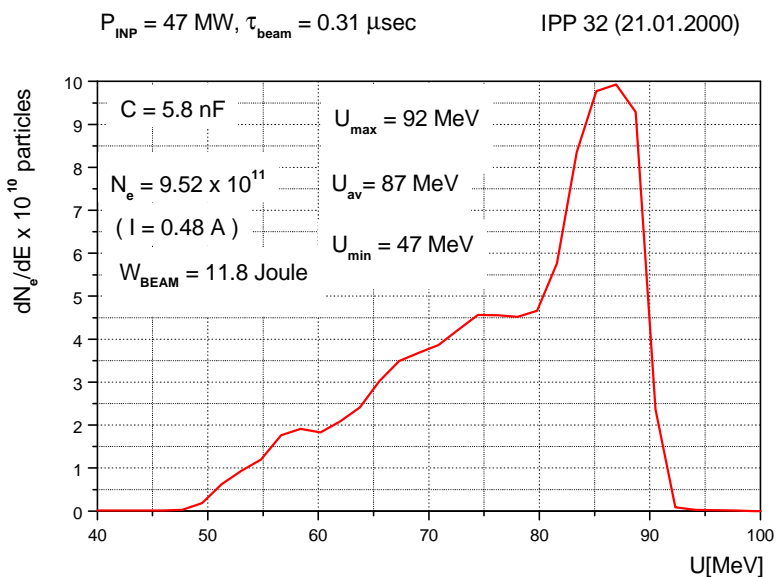


Fig.15. Particle density distribution in a beam vs. energy.

$$W_{BEAM} = \sum_{i=1}^N U_i \cdot (\Delta Q_i / e) = 11.8 \text{ J},$$

where $N = 57$ – number of BPC lamellas, ΔQ_i and U_i charge on i -th lamella and corresponding energy.

Besides, the level of RF power transferred to the load after the AS (see Fig.16) was measured with and without beam load. Also current pulse profiles from the gun, obtained from the wall current monitor, are shown in that figure. Current profiles are slightly distorted by the reactive resistance of the transducer. It is seen, taking into account distortions, that the gun current pulse is of rectangular shape with the width $\tau_B = 310$ ns.

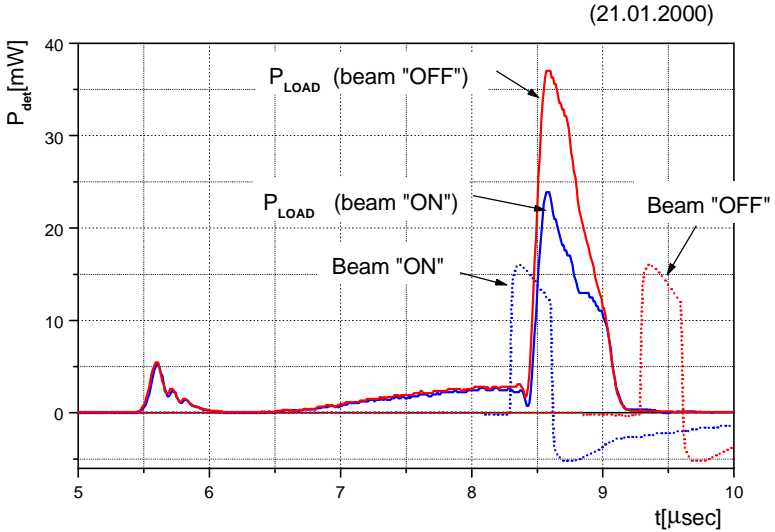


Fig. 16. The shape of RF power transferred to the load with and without beam load. The signals of current pulse from the gun wall current monitor.

The RF signal level decrease is caused by the use of the RF power fraction by the beam for its acceleration, and presence of the bunch radiation field.

By the RF pulse shape at the AS input after the system of pulse compression (see fig. 17), and AS parameters, one can completely restore the accelerating field amplitude distribution by the AS input pulse at different instants:

$$E_{gen}(z, t) = \sqrt{2R_{sh}\alpha \cdot P_0 SLED} \left(t - \frac{z}{v_{gr}} \right) e^{-\alpha z},$$

where R_{sh} AS shunt impedance,

α dissipation ratio,

$P_0 SLED(t) = P_{SLED}(0, t)$ RF power at the AS input when $z = 0$.

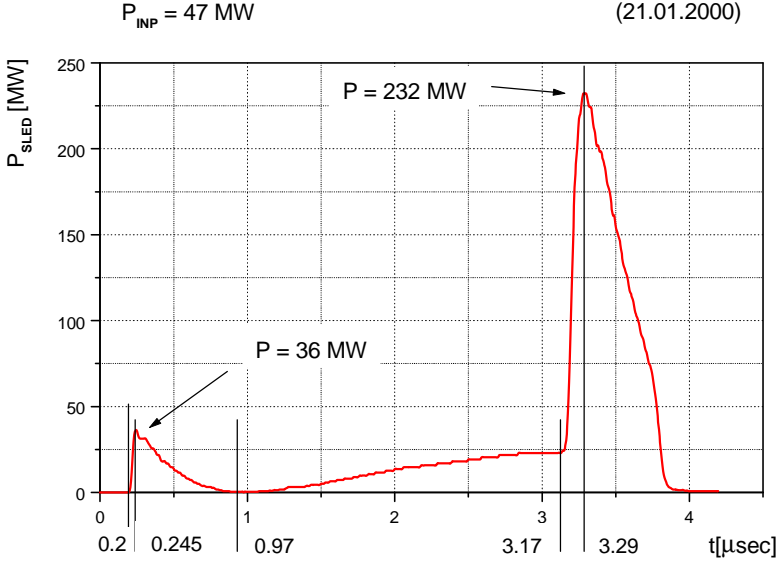


Fig.17. RF power distribution at the AS input.

To set the current at the AS input as the rectangular pulse with the amplitude I_0 and width τ_b , one can calculate the distribution of bunch radiation field along the AS as a function of time $E_b(z, t)$. For the current pulse width $\tau_b < T_f$, where T_f AS filling time by RF power, $E_b(z, t)$ is (see Fig.18):

$$E_b(z, t) = R_{sh} I_0 \cdot \frac{\sin\left(\frac{\Psi}{2}\right)}{\left(\frac{\Psi}{2}\right)} \cdot \begin{cases} 0 & \text{at } t < t_b \\ 1 - e^{-\alpha z} & \text{at } 0 < z < (t - t_b) \cdot v_{gr} \\ 1 - e^{-\frac{t - t_b}{\tau_{0.1}}} & \text{at } (t - t_b) v_{gr} < z < L = T_f v_{gr} \end{cases}$$

- where t_b time of bunch entrance into the AS,
 $\tau_{0,A}$ AS time constant,
 v_{gr} group velocity,
 Ψ bunch phase length.

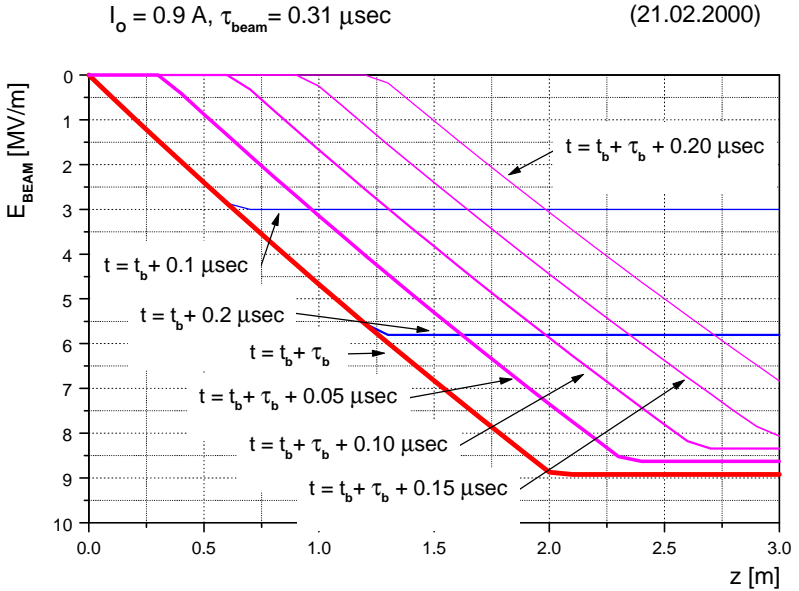


Fig.. 18. Amplitude of bunch radiation field distribution along the AS.

Total accelerating field is a sum of these two fields:

$$E_{tot}(z, t) = E_{gen}(z, t) \cdot \cos(\theta) - E_b(z, t),$$

where θ phase shift of klystron RF field relative to the bunch center.

Let us assume that particles, passed through the AS with high accelerating gradient, are bunching around $\theta = 0^\circ$. The accelerating field distribution in the AS at different time with beam load and without beam load is shown in Fig. 19 (in the figure t_{OPTIM} is the initial time of bunch entrance in the AS, corresponded to the maximum energy capacity of the beam).

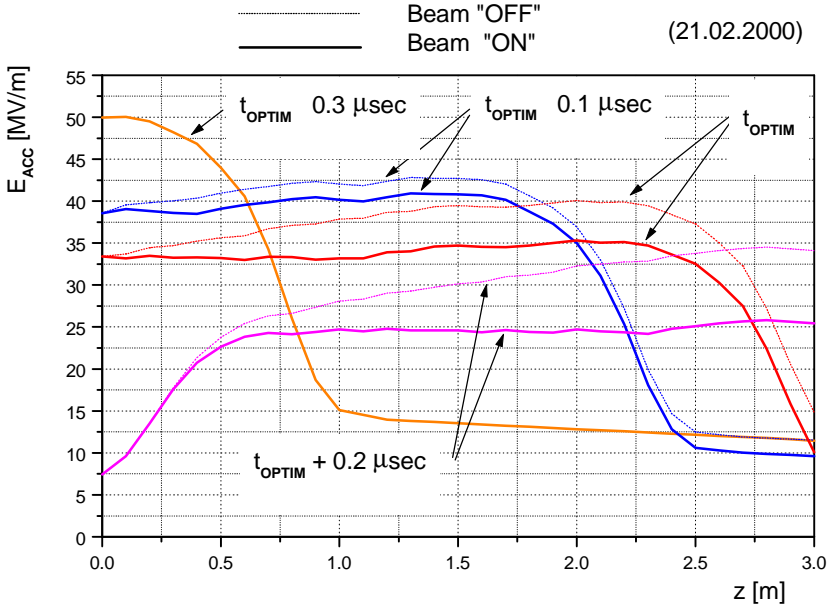


Fig.19. Accelerating field distribution in the AS at different instants.

By the field distribution along the AS, one can find the dependence of energy gain for accelerating particle on the time of entrance:

$$U(t) = e \int_0^L E_{tot}(z, t) dz .$$

The output energy of particles vs. the time of entrance is shown in Fig. 20. Top curve corresponds to the section without the beam load, middle curve loaded beam, passing the first section only, bottom curve loaded beam, passing the first and second AS (note that second section is free of RF power).

By the distribution of accelerating field along the section, one can find the power at the first section output at different time. The mentioned above dependencies, experimentally obtained (thick lines) and calculated by the given shape of input signal and beam current I_0 (thin lines) are shown in Fig 21.

$P_{INF} = 47 \text{ MW}$, $I_0 = 0.9 \text{ A}$, $\tau_{beam} = 0.31 \mu\text{sec}$ (21.01.2000)

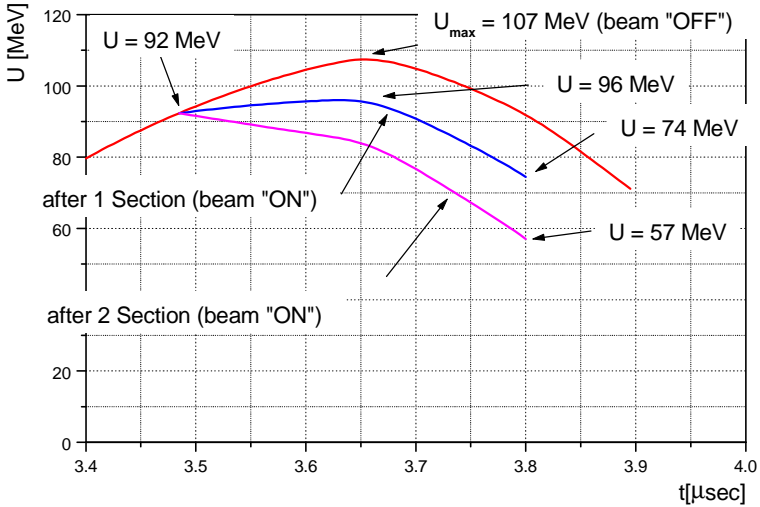


Fig. 20. Output energy of particles vs. time of entrance.

By the experimental dependencies of the output power with and without beam load, one can derive the dependence of bunch radiation field at the AS output on time:

$$\Delta E_b(t) = \sqrt{2R_{sh}\alpha} \cdot \left(\sqrt{P_{Load}(beam\ "OFF")(t)} - \sqrt{P_{Load}(beam\ "ON")(t)} \right) .$$

When the bunch of rectangular shape, width τ_b and amplitude I_0 , passes through the accelerating section, the following distribution of bunch radiation field amplitude will be at the output of AS at different time:

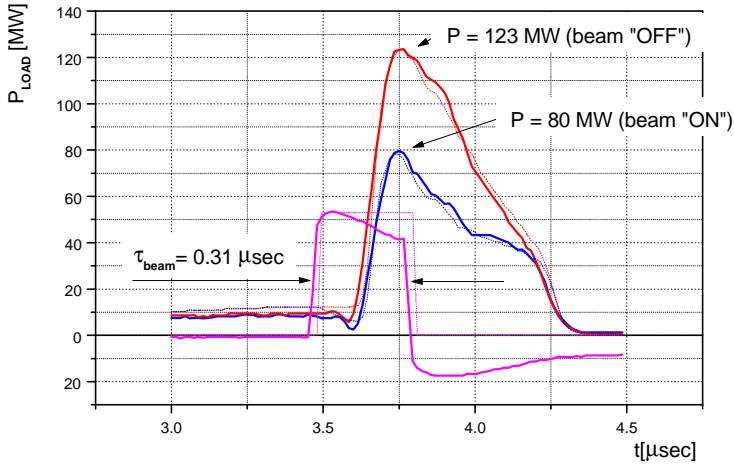


Fig. 21. Output power in the first section vs. time.

$$E_b(L, t) = R_{sh} I_0 \cdot \frac{\sin\left(\frac{\Psi}{2}\right)}{\left(\frac{\Psi}{2}\right)} \cdot \begin{cases} 0 & 0 < t < t_b \\ 1 - e^{-\frac{t-t_b}{\tau_{0,A}}}, & t_b < t < t_b + \tau_b \\ 1 - e^{-\frac{t-t_b}{\tau_{0,A}}} - 1 + e^{-\frac{t-t_b-\tau_b}{\tau_{0,A}}}, & t_b + \tau_b < t < t_b + T_f \\ e^{-\frac{t-t_b-\tau_b}{\tau_{0,A}}} - e^{-\alpha L}, & t_b + T_f < t < t_b + \tau_b + T_f \\ 0 & t_b + \tau_b + T_f < t \end{cases}$$

where t_b initial time of bunch entrance into AS,

τ_b bunch width,

T_f filling time of the AS.

The experimental and calculated dependencies of bunch radiation field at the output of the AS are shown in Fig. 22.

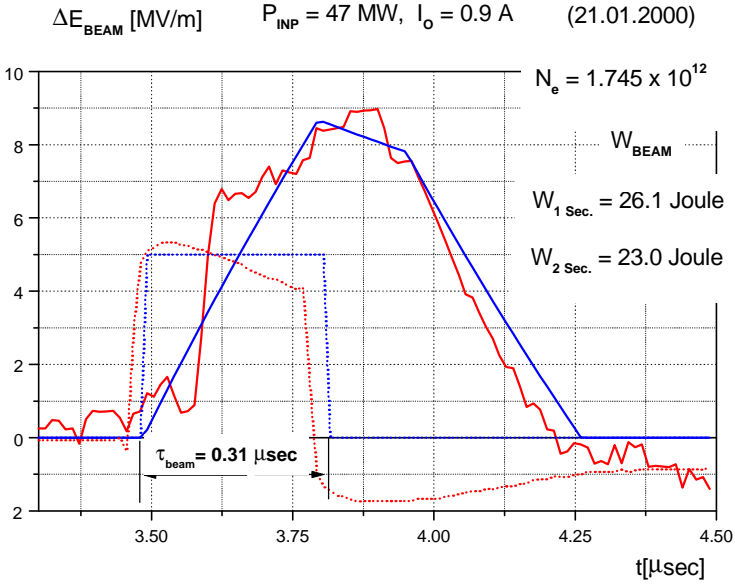


Fig. 22. Radiation field amplitude at the output of first AS vs. time.

It is seen, that at different time they are hard enough to compare. Because integral comparison was carried out, i.e. integrals over time were compared along the experimental curve

$$Int_1 = \int_0^{\infty} \Delta E_b(L, t) dt = \int_{t_b}^{t_b + \tau_b} \Delta E_b(L, t) dt$$

and along the calculated curve

$$Int_2 = \int_{t_b}^{t_b + \tau_b} E_b(L, t) dt = R_{sh} Q \cdot \frac{\sin\left(\frac{\Psi}{2}\right)}{\frac{\Psi}{2}} \cdot (1 - e^{-\alpha \cdot L}),$$

where $Q = I_0 \cdot \tau_b$ total bunch charge.

To compare these integrals and to take into account the maximum energy measured by BPC ($U_{max} = 92 \text{ M}\text{\AA}\text{B}$), the total charge of the beam accelerated in the first AS $Q = 2.8 \cdot 10^{-7} \text{ Coulomb}$, and the value of input RF power $P_{INP} = 47 \text{ MW}$ were calculated. Then total number of particles in the pulse

$$N_e = Q / e = 1.75 \cdot 10^{12},$$

and pulsed beam current is

$$I_0 = \frac{Q}{\tau_b} = 0.9 \text{ A}.$$

The energy capacity of the beam after the first section is:

$$W_{1\text{Sec.}} = \int_{t_b}^{t_b + \tau_b} U_1(P_{INP}, I_0, t) dN_e(t) = \frac{I_0}{e} \int_{t_b}^{t_b + \tau_b} U_1(P_{INP}, I_0, t) dt = 26.1 \text{ J},$$

where $U_1(P_{INP}, I_0, t)$ is dependence of beam energy gain after the first AS on the time of entrance in the AS. The beam energy capacity after the second AS (free of RF power), with the constraint that the beam passes through the AS without losses, is:

$$W_{2\text{Sec.}} = \frac{I_0}{e} \int_{t_b}^{t_b + \tau_b} U_2(P_{INP}, I_0, t) dt = 23 \text{ J},$$

where $U_2(P_{INP}, I_0, t) = U_1(P_{INP}, 2 \cdot I_0, t)$ dependence of beam energy gain after acceleration in the first AS and passing the second AS on the time of entrance in the AS.

The measured pulsed current from the electron gun is $I_G = 2.6 \text{ A}$, that corresponds to the number of electrons in the pulse of $N_e = 5.2 \cdot 10^{12}$ at pulse width $\tau_b = 310 \text{ ns}$. The calculated number of particles after the acceleration in the first section is $N_e = 1.75 \cdot 10^{12}$. Thus, around 66% of particles are lost in this experiment due to RF buncher is switched off.

Note, that BPC after the second section measured of $N_e = 0.95 \cdot 10^{12}$ particles in the pulse, i.e. about half of the accelerated beam was lost in the second section. The cause is now settling.

The accelerator of IREN project consists of two accelerating assemblies, each one includes: 5045 klystron, SLED type system of power compression and one accelerating section [4]. The project operational conditions and parameters of the accelerating beam after the first AS, beam parameters obtained in the experiments described above, and converting of these parameters for klystron

output power $P_{kl} = 63$ MW and pulse repetition rate $F = 150$ Hz is presented in Table 6. That corresponds to project operational conditions of the accelerator for IREN

Table 6.

		IREN	Exp.	Conv.
klystron output power	P_{kl} [MW]	63	47	63
pulse repetition rate	F [Hz]	150	2.5	150
pulsed current	I_0 [A]	1.5	0.9	1.5
pulse current width	τ_b [ns]	250	310	250
beam energy	U_{beam} [MeV]	105	92	105
beam energy capacity	W_{beam} [J]	40	26	38.6
beam mean power	$P_{beam\ av.} = W_{beam} \cdot F$ [kW]	6		5.8

As table shows, by the use of the system of pulse compression, accelerating section and RF load developed for VEPP 5 pre injector, it is possible to construct accelerator satisfied of the IREN project requirements. At that, the beam at the output of first accelerating section will have the energy distribution shown in Fig.23. As it is seen, in relation to beginning time of electron gun current pulse one may obtain the beam with low energy spread at the output of the accelerating section (bottom curve is $\Delta U \approx 7$ MeV). The average beam power will be slightly less than the maximum one (middle curve).

Conclusion

Performed tests showed that the accelerating sections, produced due to developed and realized in INP technology, have high electric strength – accelerating gradient in the AS is reached more than 50 MeV/m (average accelerating gradient up to 35 MeV/m). That exceeds the project parameters of VEPP 5 pre injector accelerated sections. Tests with the long bunch proved the AS operation at high current load with a high power beam, such as in the project of accelerator for IREN.

References

- [1] A.V. Aleksandrov et al., "Preinjector for electron positron factories". Proc. 1994 XIV Conf. on Charge Part. Acc., Protvino, Russia.
- [2] A.V. Aleksandrov et al., "Electron positron preinjector of VEPP 5 complex" Proceedings of the XVIII International Linear Accelerator Conference,

26 30 August 1996, Geneva, Switzerland, Vol. 2, pp. 821 823.

[3] Отчет о научно-исследовательской работе (договор N 92-4) "Линейный ускоритель электронов для интенсивного источника резонансных нейтронов (ИРЕН)", Новосибирск, 1993.

[4] V. Antropov et. al., "IREN test facility at JINR". Proceedings of the XVIII International Linear Accelerator Conference, 26 30 August 1996, Geneva, Switzerland, Vol. 2, pp. 505 508.

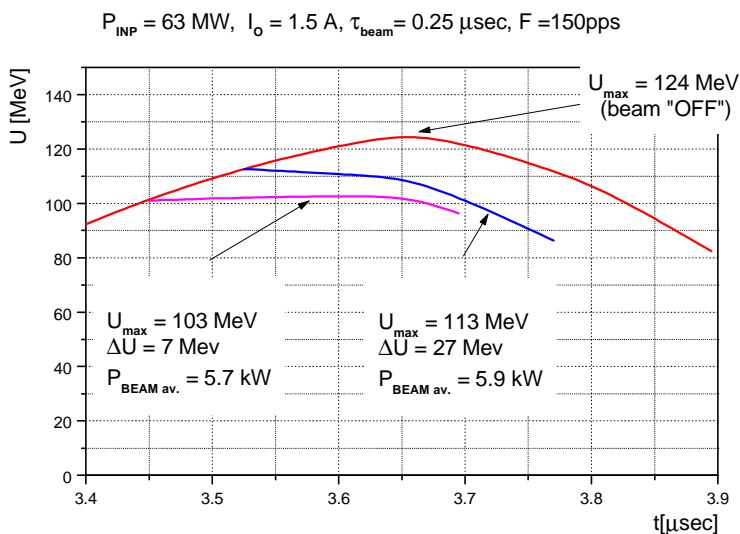


Fig.23. Electrons output energy vs. time of entrance of electrons in the AS.